

SUPPLEMENTARY INFORMATION

Formation of a uranyl hydroxide hydrate via hydration of $[(\text{UO}_2\text{F}_2)(\text{H}_2\text{O})]_7 \cdot 4\text{H}_2\text{O}$

Marie C. Kirkegaard, Tyler L. Spano, Michael W. Ambrogio, J. L. Niedziela, Andrew Miskowiec, Ashley E. Shields, and Brian B. Anderson

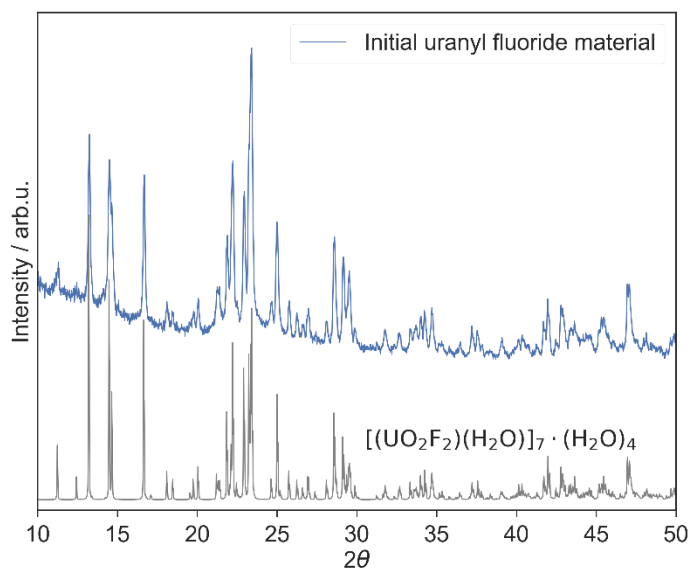


Figure S1: XRD pattern of the initial uranyl fluoride material, identified as $[(\text{UO}_2\text{F}_2)(\text{H}_2\text{O})]_7 \cdot 4\text{H}_2\text{O}^1$ with no noticeable impurities.

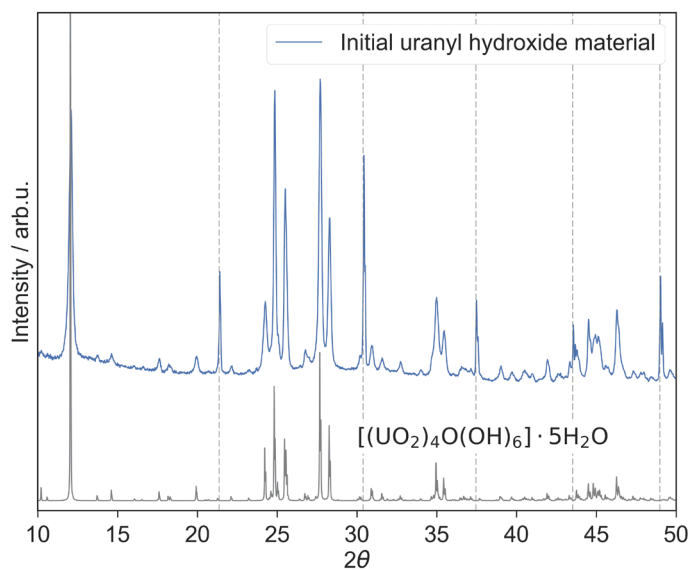


Figure S2: XRD pattern of the initial uranyl hydroxide material, identified as synthetic metaschoepite, $[(\text{UO}_2)_4\text{O}(\text{OH})_6] \cdot (\text{H}_2\text{O})_6^2$ with no noticeable impurities.

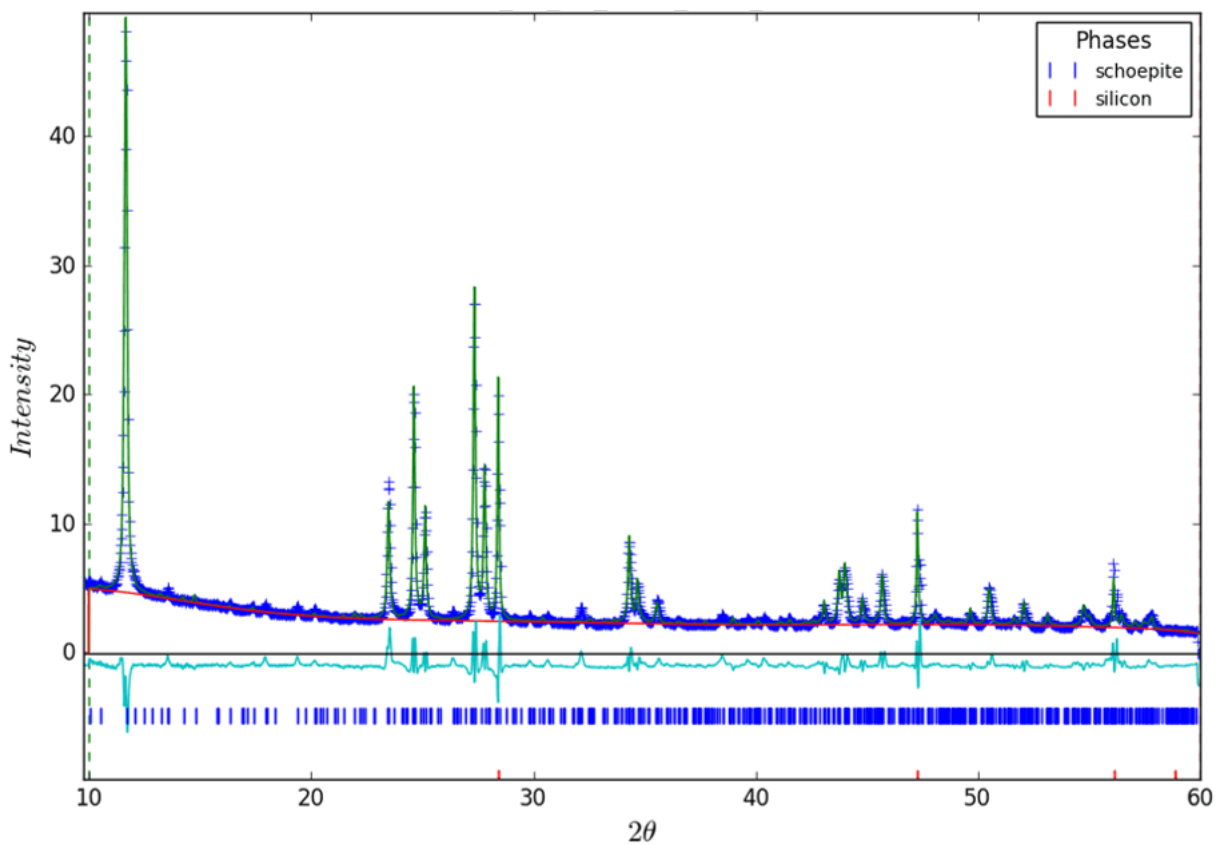


Figure S3: Rietveld refinement of the uranyl hydroxide product using the crystal structure of schoepite.³ Silicon powder was added to the sample as a standard.

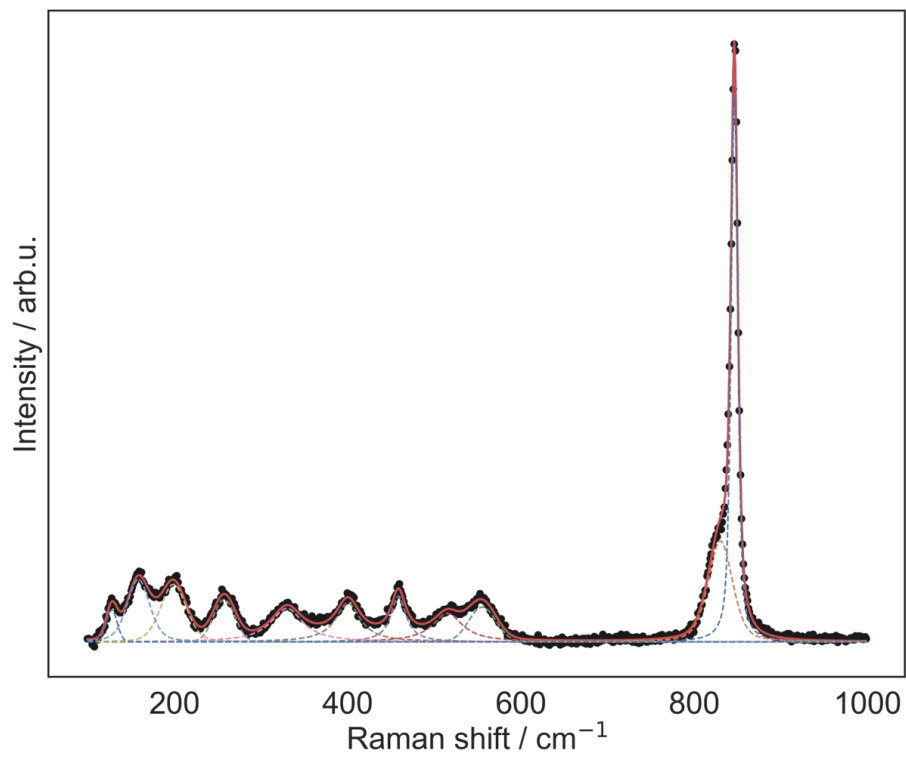


Figure S4: Pseudo-Voigt fits of the Raman peaks of the uranyl hydroxide product.

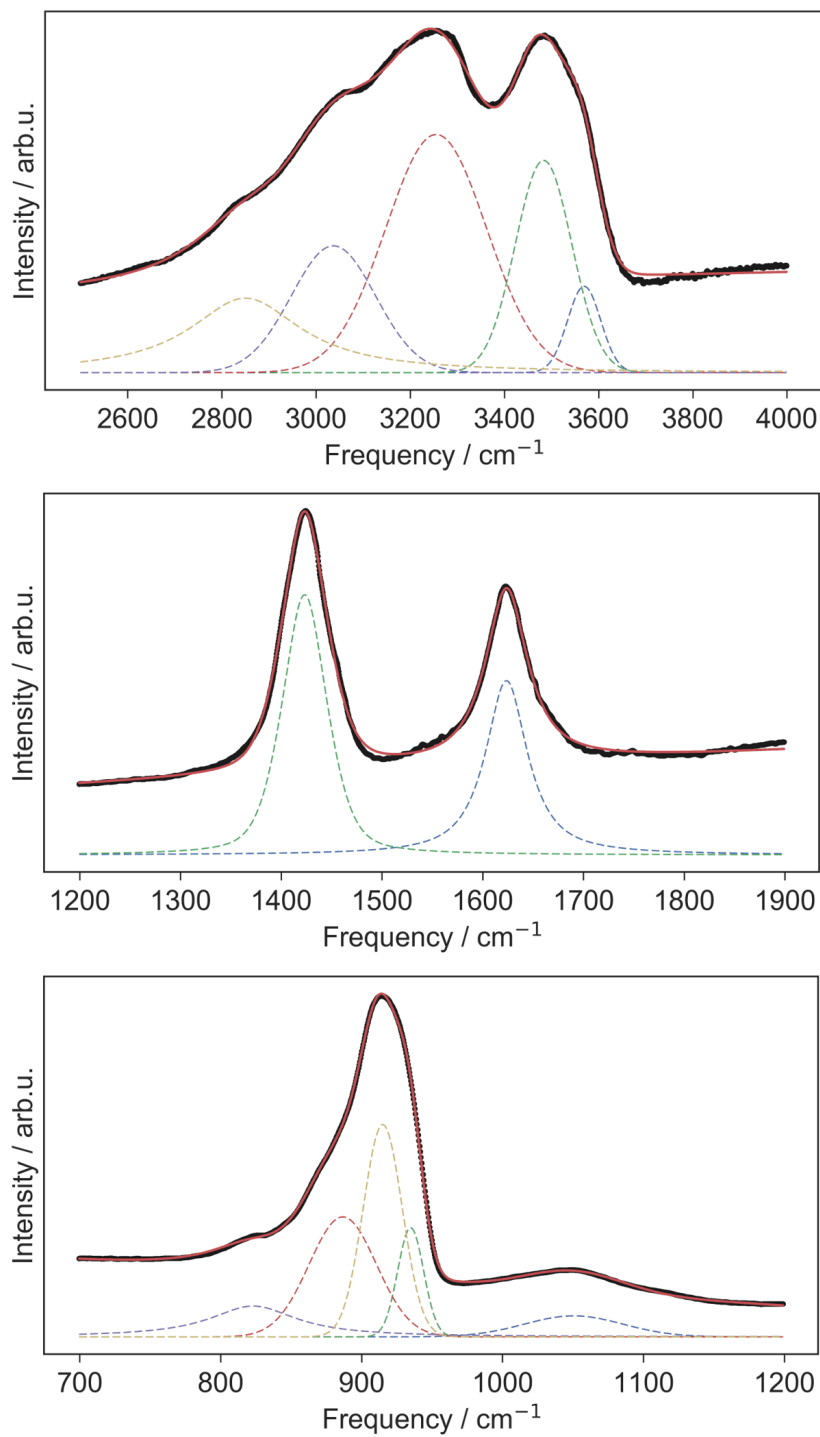


Figure S5: Pseudo-voigt fits of the IR peaks of the uranyl hydroxide product.

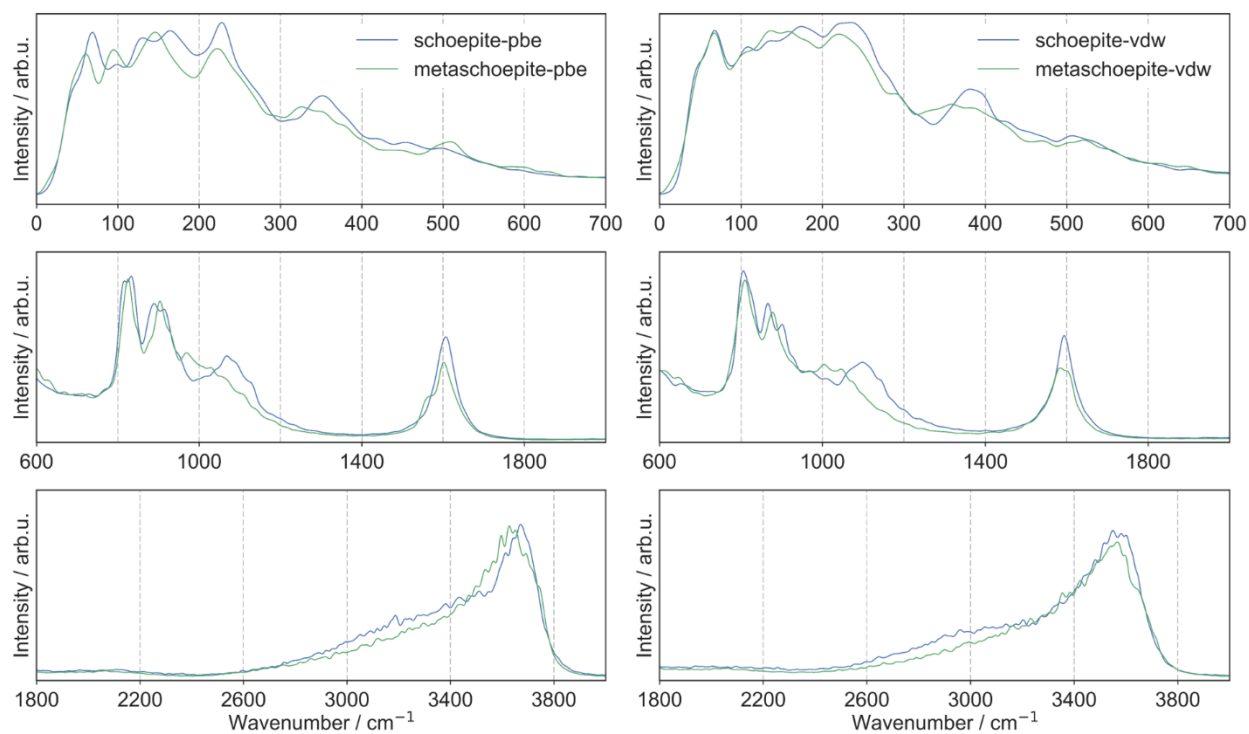


Figure S6. Comparison of the power spectra of schoepite and metaschoepite calculated from *ab initio* molecular dynamics simulations. Experimental details for the PBE simulation of metaschoepite are described in Kirkegaard *et al.* 2019.⁴ The remaining simulations were conducted in the same manner, using either the PBE (CITE) functional or optb86-vdW (CITE) functional. In both cases, the U-O-H bending mode near 1000 cm^{-1} is demonstrated to be the most sensitive to the differences between schoepite and metaschoepite.

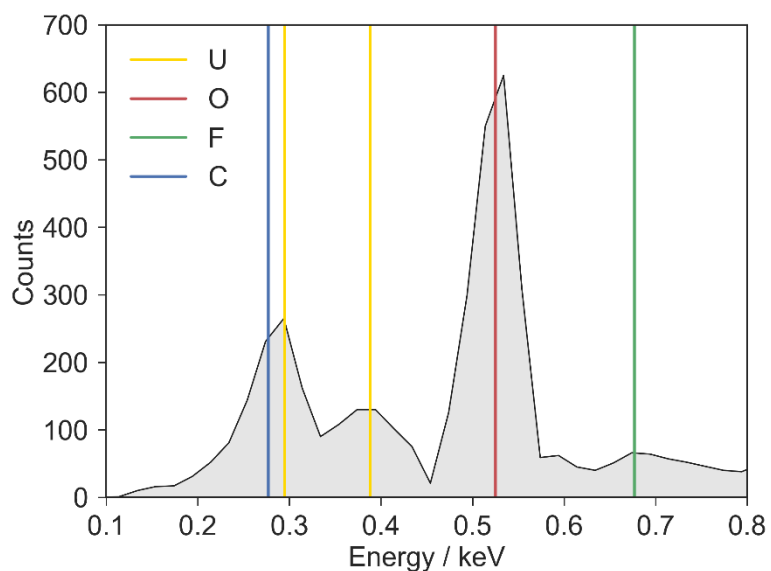


Figure S7: Lower energy region of the SEM-EDS spectrum of a representative particle of the uranyl hydroxide product on a silicon substrate. It is difficult to make a definitive conclusion regarding the presence of carbon in this sample due to the overlap of the carbon K_{α} peak (expected at 0.28 keV) and a satellite uranium peak near 0.29 keV. Carbon was not identified as a component species in the EDS spectral matching software.

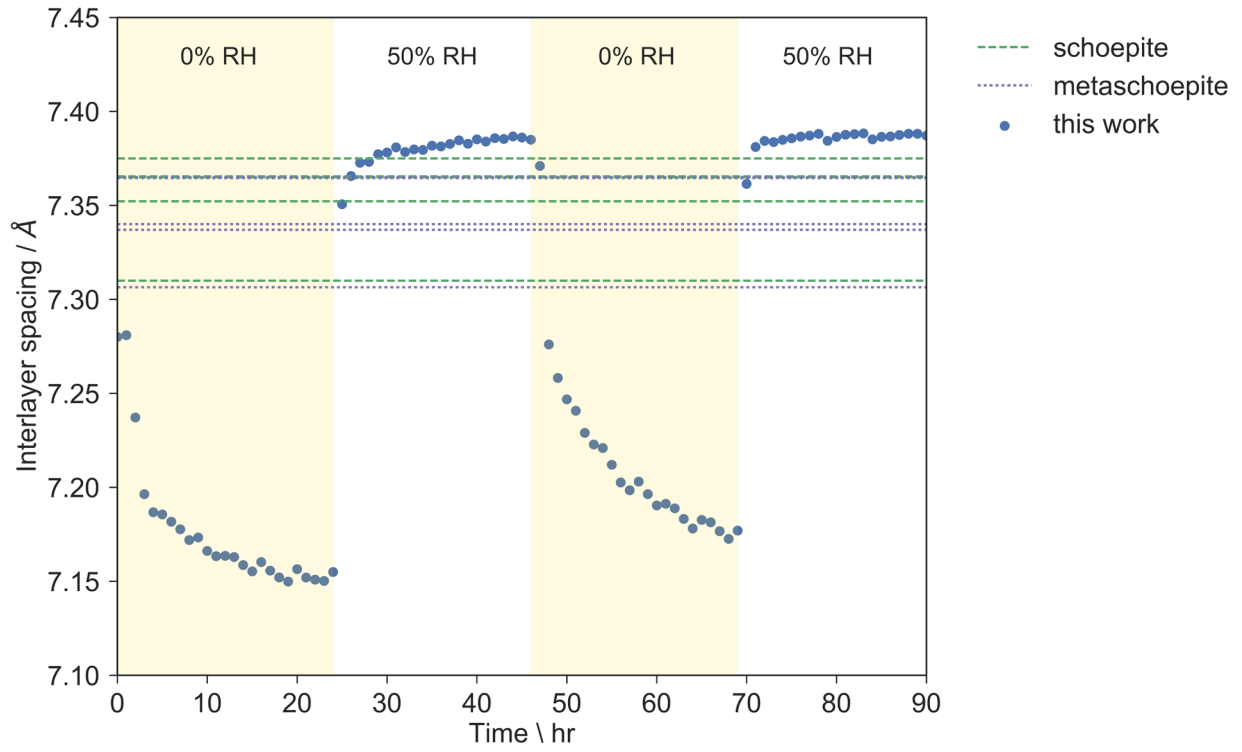


Figure S8

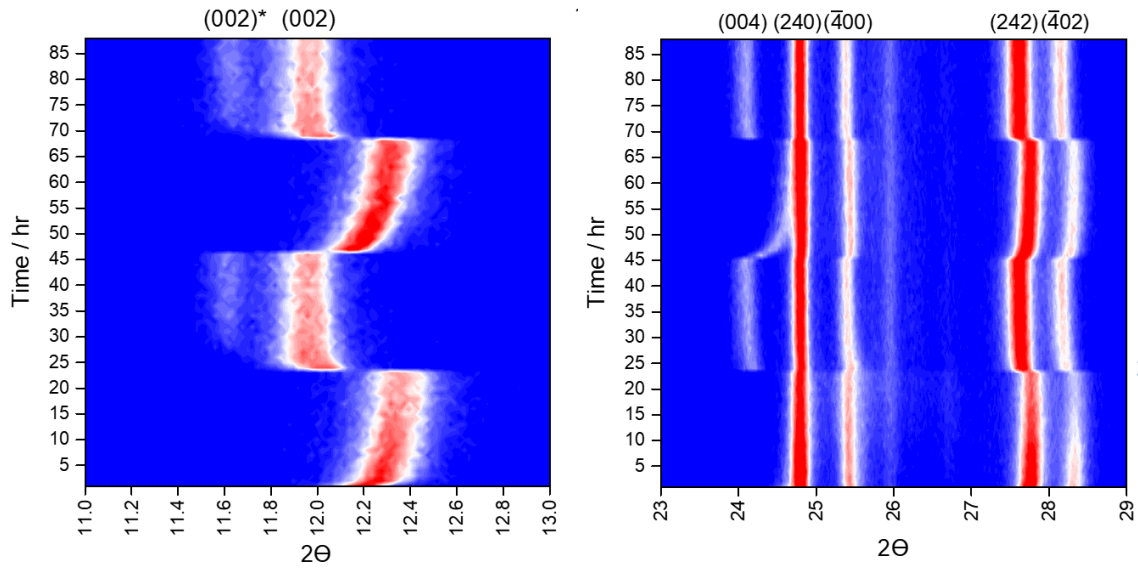


Figure S9

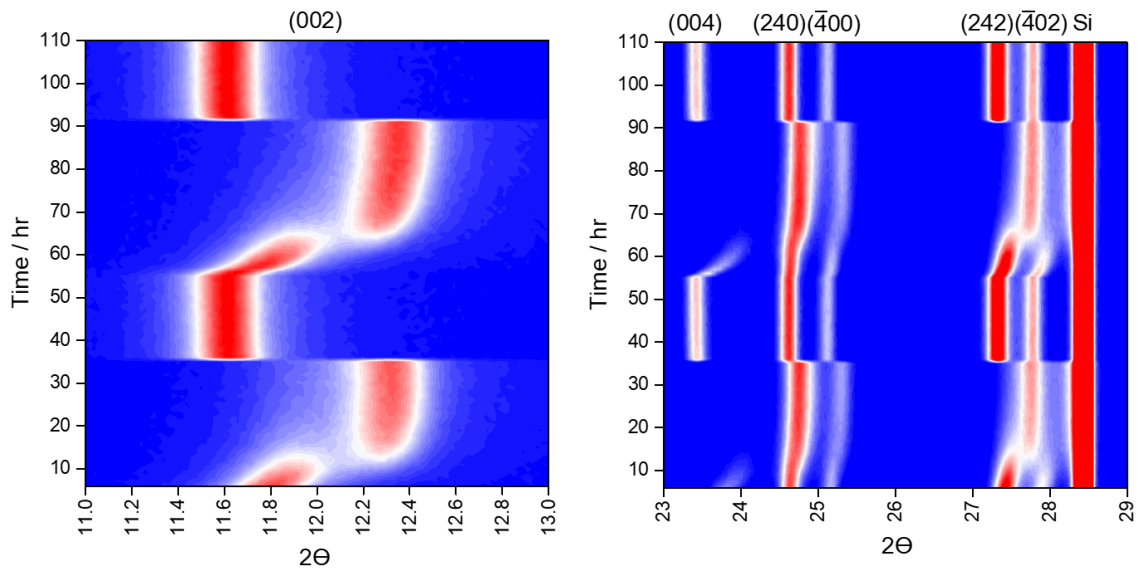


Figure S10

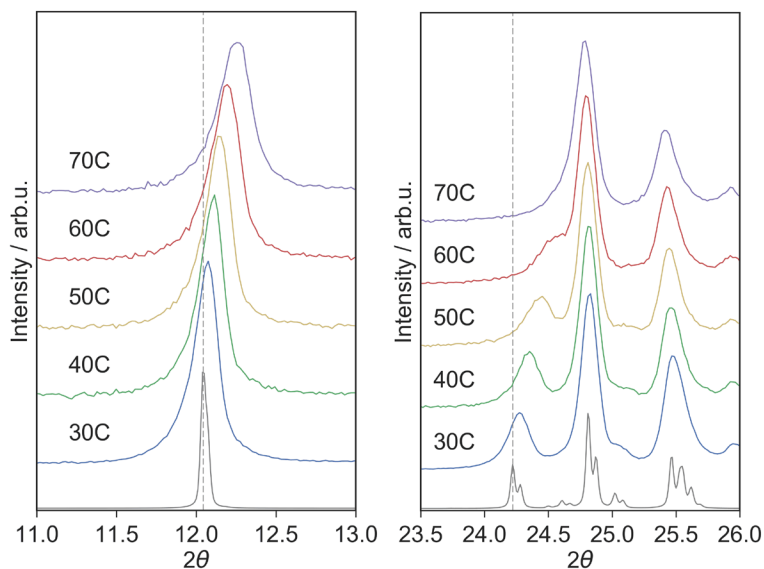


Figure S11. Regions of the XRD pattern of synthetic metaschoepite at increasing temperature, showing shifts in the (left) (002) reflection, and (right) (004) reflection. Dashed lines at $2\vartheta=12.043^\circ$ and $2\vartheta=24.2216^\circ$ show the expected location of the (002) and (004) reflections, as determined by Weller *et al.*²

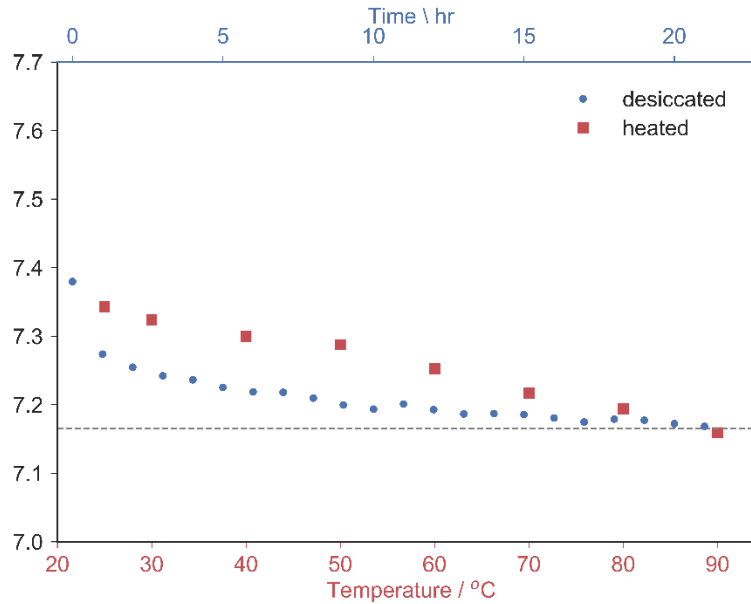


Figure S12. Interlayer spacing of synthetic metaschoepite as a function of temperature (red squares) and as a function of desiccation time (blue circles). The dashed line at 7.165 Å shows the approximate minimum layer spacing upon desiccation and upon heating before a discrete phase transition occurred >90 °C.

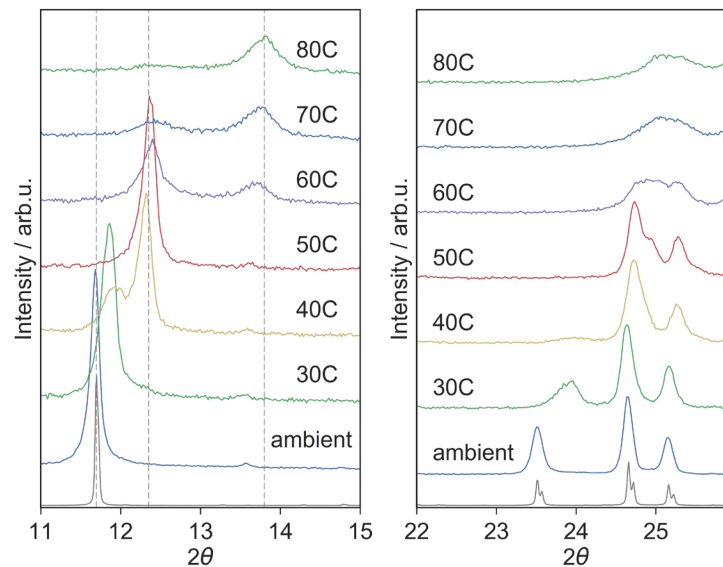


Figure S13. Regions of the XRD pattern of the uranyl hydroxide product at increasing temperature, showing shifts in the (left) (002) reflection, and (right) (004) reflection.

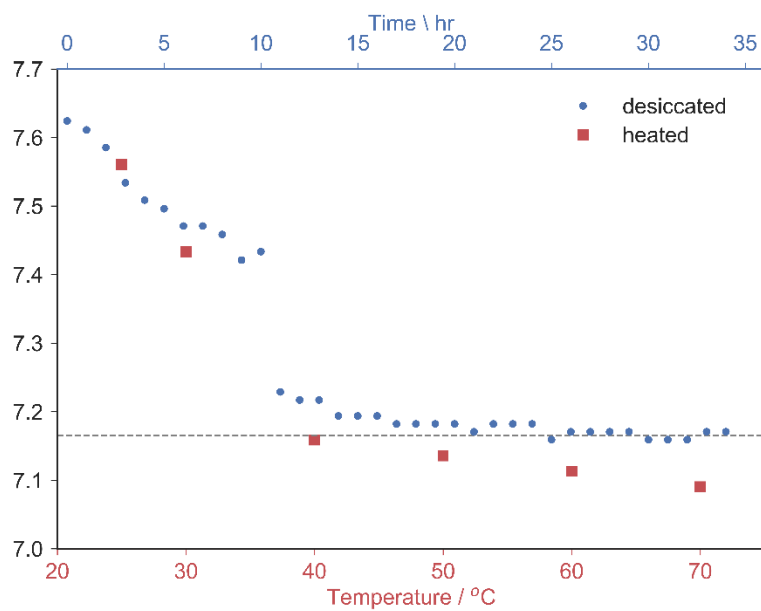


Figure S14. Interlayer spacing of the uranyl hydroxide product as a function of temperature (red squares) and as a function of desiccation time (blue circles). The dashed line at 7.165 Å shows the approximate minimum layer spacing upon desiccation.